Acta Crystallographica Section D
Biological Crystallography
ISSN 0907-4449

Crystallization and preliminary X-ray analysis of *Yersinia pseudotuberculosis*-derived mitogen

Roberta Donadini,[a] Malin Wåhlberg,[a]† Takao Kohsaka,[b]‡ Yasuhiko Ito[b]§ and Barry A. Fields[a]*

[a]School of Molecular and Microbial Biosciences, University of Sydney, NSW 2006, Australia, and [b]Department of Allergy and Immunology, National Children's Medical Research Center, 3-35-31 Taishido, Setagaya-ku, Tokyo 154-8509, Japan

† Present address: AstraZeneca R&D Mölndal, S-431 83 Mölndal, Sweden.
‡ Present address: Department of Gastroenterology, National Center for Child Health and Development, 2-10-1 Okura, Setagaya-ku, Tokyo 157-8535, Japan.
§ Present address: Kurume Research Park Co. Ltd, 2432-2 Aikawamachi, Kurume, Fukuoka 839-0861, Japan.

Correspondence e-mail: b.fields@mmb.usyd.edu.au

Received 12 February 2003
Accepted 14 May 2003

Yersinia pseudotuberculosis-derived mitogen (YPM), a superantigen with no amino-acid sequence similarity to other known superantigens, has been crystallized by the sitting-drop vapour-diffusion method. The crystals belong to space group $C2$, with unit-cell parameters $a = 138.67$, $b = 78.66$, $c = 32.91$ Å, $\beta = 91.97^\circ$. A native data set has been collected to a resolution of 1.8 Å using synchrotron radiation. Self-rotation function calculations suggest the presence of three molecules in the asymmetric unit, corresponding to a solvent content of 45%.

1. Introduction

Superantigens (SAgs) are viral or bacterial proteins that target the immune system and activate up to 30% of the total T-cell population (Kotzin *et al.*, 1993). In contrast, conventional antigens bound as peptide fragments to major histocompatibility complex (MHC) molecules typically activate only one in 10^5–10^6 T cells. The simultaneous binding of SAgs to the T-cell antigen receptor (TCR) on T cells and to MHC molecules on antigen-presenting cells enables the highly specific mode of T-cell antigen recognition to be bypassed. The clinical hallmarks of SAg-mediated immunostimulation (*e.g.* fever, rash and hypotension) are attributed to the massive release of inflammatory cytokines resulting from the activation of such a large fraction of the T-cell pool. SAgs are active agents in staphyloccocal food poisoning (Dinges *et al.*, 2000) and staphylococcal and streptococcal toxic shock syndrome (Dinges *et al.*, 2000; McCormick *et al.*, 2001). SAgs have also been implicated in the pathogenesis of a growing number of other diseases, including inflammatory bowel diseases (*e.g.* Crohn's disease and ulcerative colitis; McKay, 2001), inflammatory skin diseases (*e.g.* psoriasis and atopic dermatitis; Skov & Baadsgaard, 2000) and vasculitis and related disorders such as Kawasaki disease (Tervaert *et al.*, 1999). SAgs have also been implicated as playing a role in some autoimmune disorders such as multiple sclerosis and rheumatoid arthritis (Schiffenbauer *et al.*, 1998; Macphail, 1999).

The pyrogenic superantigens from *Staphylococcus aureus* and *Streptococcus pyogenes* have been the most extensively studied and crystal structures have been determined for several of these SAgs and their complexes with the T-cell antigen receptor and major histocompatibility complex (MHC) molecules (reviewed in Fraser *et al.*, 2000; Papageorgiou & Acharya, 2000; Sundberg *et al.*, 2002). Viral superantigens are not as well characterized as the bacterial SAgs; however, interest in viral SAgs has been heightened recently by the discovery that human endogenous retrovirus HERV-K18 is a superantigen that is transcriptionally activated by Epstein–Barr virus (Sutkowski *et al.*, 2001). *Yersinia pseudotuberculosis*-derived mitogen, the only known SAg produced by a Gram-negative bacterium, may play an important role in the pathogenesis of *Y. pseudotuberculosis* infection, the symptoms of which can include fever, rash, diarrhoea, vomiting and arthritis (Abe *et al.*, 1997). *Y. pseudotuberculosis*, a food-borne pathogen, may also play a role in the pathogenesis of Kawasaki disease, the most common form of childhood-acquired heart disease in developed countries (Konishi *et al.*, 1997; Freeman & Shulman, 2001). YPM has no significant sequence homology with any other known protein and its molecular weight of 14 kDa is much lower than that of other SAgs (*e.g.* 25 kDa for staphylococcal enterotoxins). We report the first crystallization and X-ray diffraction studies of YPM.

2. Materials and methods

2.1. Expression and purification

YPM was overexpressed from a pMAL-p2X vector (New England Biolabs) as a maltose-binding protein (MBP)-His_{10}-YPM fusion protein in the periplasm of *Escherichia coli* Novablue cells using a method based on that of Ito *et al.* (1999). Briefly, transformed *E. coli* were cultured in 10 ml of Luria–Bertani medium (LB) containing 100 µg ml^{-1} ampicillin and 10 µg ml^{-1} tetracycline at 310 K for 4–6 h. This culture was added to 700 ml of fresh LB/ampicillin/tetracycline and the culture was grown overnight. The overnight culture was added to 9 l of fresh LB/ampicillin/tetracycline

and grown until the optical density at λ = 600 nm reached 0.5–0.6. Protein expression was induced by the addition of isopropyl thio-β-D-galactoside (IPTG) to a final concentration of 0.3 m*M*. 3 h after induction, the culture was harvested by centrifugation and the cells were suspended in 1 ml of lysis buffer [20 000 U of polymixin B sulfate (Sigma) in phosphate-buffered saline (PBS)] per gram of wet cell paste. The suspension was agitated gently for 30 min at 310 K and centrifuged to obtain the periplasmic contents in the supernatant. The MBP-His_{10}-YPM fusion protein was purified using His-Bind resin according to the manufacturer's instructions (Novagen). The fusion protein was desalted and concentrated using Centriplus-30 and Centricon-30 concentrators with PBS as solvent. YPM was cleaved from the fusion protein by digestion with factor Xa (New England Biolabs) at 293 K for 48–72 h (enzyme:substrate ratio = 1:400–1000). YPM was separated from MBP by recycling through His-Bind resin. The protein was further purified using gel-filtration (Superdex G-75, Pharmacia), anion-exchange (Mono Q, Pharmacia) and hydrophobic interaction chromatography (hydroxyapatite media, Bio-Rad Laboratories).

Selenomethionine-substituted (SeMet) YPM was expressed using the method of methionine-pathway inhibition (Doublié, 1997). The protocol was similar to that used for the native protein except that the growth and overexpression procedures were modified as follows: transformed *E. coli* were cultured in 2.6 l of LB media to an optical density at λ = 600 nm of 0.2–0.4. Cells were then harvested by centrifugation, washed thoroughly in minimal media and recentrifuged. The cell pellet was resuspended into 2.6 l of minimal media that had been supplemented with 4 g l^{-1} glucose, 10 m*M* $MgSO_4$, 50 mg l^{-1} thiamine, 150 mg l^{-1} L-threonine, L-phenylalanine and L-lysine and 75 mg l^{-1} L-valine, L-leucine, L-isoleucine and L-selenomethionine. The culture was incubated for 30 min before induction with IPTG and then grown for 12–18 h before harvesting. Purification of SeMet-substituted YPM was similar to that for native YPM, except that the anion-exchange and hydrophobic interaction chromatography steps were omitted. A 12-residue N-terminal deletion mutant of SeMet YPM was also expressed and purified. Incorporation of the single selenomethionine residue was confirmed by electrospray mass spectrometry using a Finnegan LCQ instrument (Fig. 1).

2.2. Crystallization

Crystals were grown by the sitting-drop vapour-diffusion technique at 293 K. Initial crystallization screens were performed using Hampton Research Crystal Screens I and II. Several conditions produced spherical aggregates that did not diffract. Small crystals grew from condition No. 5 of Crystal Screen II (2.0 *M* ammonium sulfate, 5% 2-propanol); however, these only diffracted to ~5 Å. After refining the conditions using ammonium sulfate and low-molecular-weight polyethylene glycol (PEG) as the precipitants, the best crystals appeared in 5–7 d and grew for a further 1–2 weeks. The reservoir contained 1.95–2.10 *M* ammonium sulfate, 4–5%(*v*/*v*) PEG 200 and 0.1 *M* sodium citrate pH 5.8–7.6. Drops typically contained 2 µl of the reservoir solution and 3 µl of YPM solution (75 mg ml^{-1} protein, 0.1 *M* sodium citrate pH 7.2). It was possible to grow crystals at lower protein concentrations at slightly slower rates. A protein concentration of 50 mg ml^{-1} was used for crystallizing SeMet YPM in order to conserve protein. The theoretical pI values of full-length YPM and the N-terminal deletion mutant are 5.1 and 5.7, respectively. Both of these values are lower than the pH range of the crystal-growth conditions.

2.3. Data collection

Crystals were cryoprotected by washing them with a Paratone-N/mineral oil mixture using a nylon loop and flash-cooling in a nitrogen-gas stream. Data from native crystals were collected at a temperature of 100 K on beamline 1-5 at the Stanford Synchrotron Radiation Laboratory (SSRL) using an ADSC Quantum-4R CCD detector. 240 diffraction images were recorded, each corresponding to oscillations of 1.5° about the φ axis, to give a total of 360° of data. The crystal-to-detector distance was 122 mm and the X-ray wavelength was 1.071 Å. Diffraction images were indexed, integrated and scaled using *DENZO* and *SCALEPACK* from the *HKL* software package (Otwinowski & Minor, 1997).

2.4. Self-rotation functions

Self-rotation function calculations were performed with the *CCP*4 program *POLARRFN* (Collaborative Computational Project, Number 4, 1994) using data in the resolution range 15–4 Å and an integration radius of 25 Å.

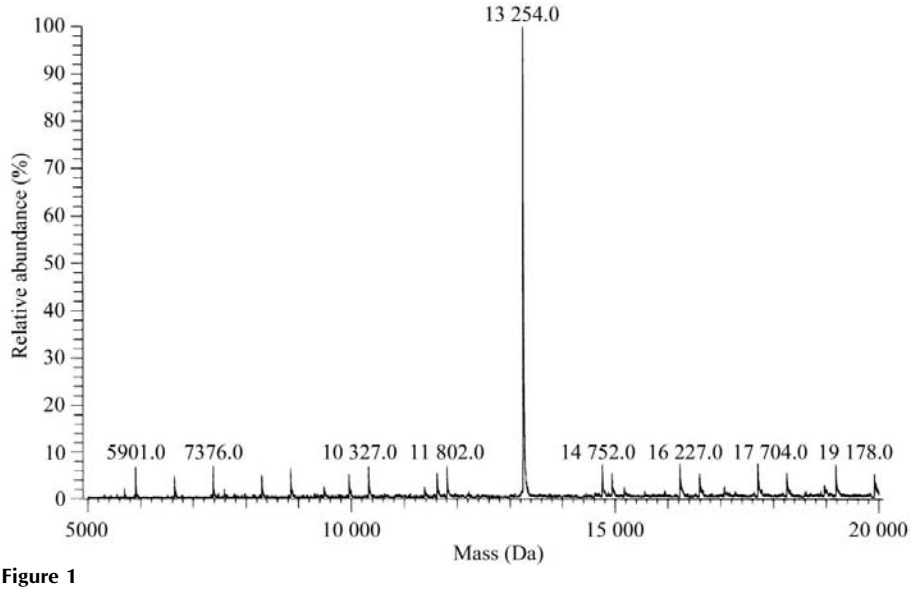

Figure 1
Mass spectrum of N-terminal deletion mutant of SeMet YPM. The mass calculated from the sequence is 13 255 Da.

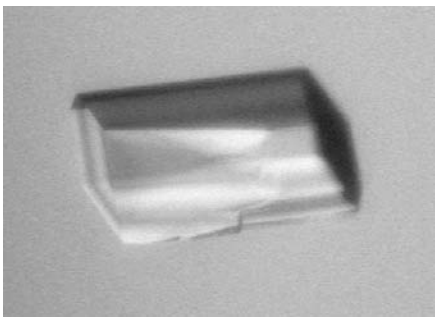

Figure 2
Native monoclinic crystal of *Y. pseudotuberculosis*-derived mitogen. The longest dimension of the crystal is ~0.4 mm.

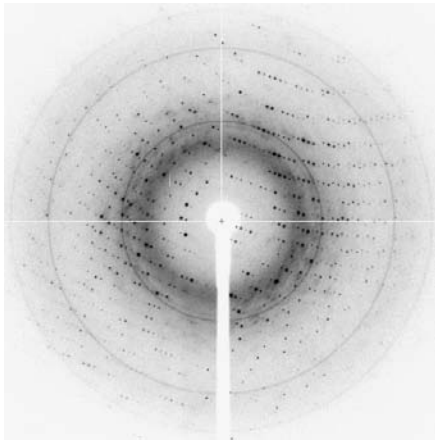

Figure 3
Diffraction image recorded on SSRL beamline 1-5 from the YPM crystal shown in Fig. 1. The oscillation range was 1.5°. The edge of the image corresponds to a resolution of 1.8 Å.

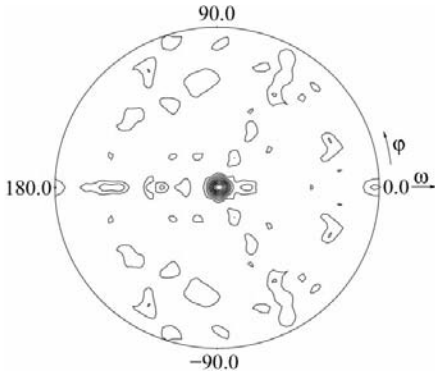

Figure 4
Self-rotation function. $\kappa = 120^\circ$ section indicating the presence of a non-crystallographic threefold axis approximately parallel to the crystallographic *c* axis. The spherical polar coordinates (φ, ω, κ) of the peak are (0.0, 89.7, 120.0).

3. Results and discussion

Crystals varied in morphology and the largest crystals measured up to 0.5 mm in the longest dimension (Fig. 2). The crystals belong to the monoclinic space group *C*2, with unit-cell parameters a = 138.67, b = 78.66, c = 32.91 Å, $\beta = 91.97^\circ$. A 99.8% complete data set with greater than sevenfold redundancy was collected to 1.8 Å resolution at SSRL. A diffraction image and data-processing statistics are shown in Fig. 3 and Table 1, respectively. The self-rotation function indicates the presence of a non-crystallographic threefold axis approximately parallel to the crystallographic *c* axis (Fig. 4). The presence of three molecules in the asymmetric unit gives a calculated solvent content of 45%.

Table 1
Diffraction data statistics to 1.8 Å (SSRL).

Values in parentheses refer to the outermost shell (1.86–1.80 Å).

Space group	*C*2
Unit-cell parameters	
a (Å)	138.67
b (Å)	78.66
c (Å)	32.91
β (°)	91.97
Solvent content† (%)	45
Observed reflections	230382
Unique reflections	31702
Data completeness (%)	99.8 (99.5)
$I/\sigma(I)$	40.5 (3.9)
$R_{\rm merge}$‡ (%)	4.4 (45.3)

† Three molecules per asymmetric unit. ‡ $R_{\rm merge} = 100\sum|I - \langle I\rangle|/\sum I$, where I is the intensity of an individual measurement of each reflection and $\langle I\rangle$ is the mean intensity of that reflection.

The majority of crystals were twinned and it was difficult to identify single crystals solely based on appearance. Typically, only one crystal in ten was suitable for data collection, which has severely hampered the search for heavy-atom derivatives. All attempts to reduce the level of twinning such as the use of additives (*e.g.* Hampton Research Additive Screens) were unsuccessful. Crystallization of SeMet-substituted YPM was slower and was achieved under the same conditions using protein expressed from a construct with 12 residues truncated from the N-terminus. This construct was made after mass spectrometry indicated that the native protein was prone to loss of a variable number (ranging from 6 to 13) of N-terminal residues during purification. Truncated SeMet YPM crystallizes in the same space group with the same unit-cell parameters as native YPM. Single crystals diffracting to at least 2.1 Å on a rotating-anode source have been stored at cryogenic temperatures for future MAD data collection.

This work was supported by The Wellcome Trust. We thank Mitchell Guss and David Langley for data collection at SSRL. SSRL is operated by the Department of Energy, Office of Basic Energy Sciences.

References

Abe, J., Onimaru, M., Matsumoto, S., Noma, S., Baba, K., Ito, Y., Kohsaka, T. & Takeda, T. (1997). *J. Clin. Invest.* **99**, 1823–1830.
Collaborative Computational Project, Number 4 (1994). *Acta Cryst.* D**50**, 760–763.
Dinges, M. M., Orwin, P. M. & Schlievert, P. M. (2000). *Clin. Microbiol. Rev.* **13**, 16–34.
Doublié, S. (1997). *Methods Enzymol.* **276**, 523–530.
Fraser, J., Arcus, V., Kong, P., Baker, E. & Proft, T. (2000). *Mol. Med. Today*, **6**, 125–132.
Freeman, A. F. & Shulman, S. T. (2001). *Curr. Opin. Infect. Dis.* **14**, 357–361.
Ito, Y., Seprenyi, G., Abe, J. & Kohsaka, T. (1999). *Eur. J. Biochem.* **263**, 326–337.
Konishi, N., Baba, K., Abe, J., Maruko, T., Waki, K., Takeda, N. & Tanaka, M. (1997). *Acta Paediatr.* **86**, 661–664.
Kotzin, B. L., Leung, D. Y., Kappler, J. & Marrack, P. (1993). *Adv. Immunol.* **54**, 99–166.
McCormick, J. K., Yarwood, J. M. & Schlievert, P. M. (2001). *Annu. Rev. Microbiol.* **55**, 77–104.
McKay, D. M. (2001). *Trends Immunol.* **22**, 497–501.
Macphail, S. (1999). *Int. Rev. Immunol.* **18**, 141–180.
Otwinowski, Z. & Minor, W. (1997). *Methods Enzymol.* **276**, 307–326.
Papageorgiou, A. C. & Acharya, K. R. (2000). *Trends Microbiol.* **8**, 369–375.
Schiffenbauer, J., Soos, J. & Johnson, H. (1998). *Immunol. Today*, **19**, 117–120.
Skov, L. & Baadsgaard, O. (2000). *Clin. Exp. Dermatol.* **25**, 57–61.
Sundberg, E. J., Li, Y. & Mariuzza, R. A. (2002). *Curr. Opin. Immunol.* **14**, 36–44.
Sutkowski, N., Conrad, B., Thorley-Lawson, D. A. & Huber, B. T. (2001). *Immunity*, **15**, 579–589.
Tervaert, J. W., Popa, E. R. & Bos, N. A. (1999). *Curr. Opin. Rheumatol.* **11**, 24–33.